

On the estimation of tyre self-aligning moment through a physical model and the trick tool

LENZO, Basilio <<http://orcid.org/0000-0002-8520-7953>>, ZINGONE, Salvatore Andrea and TIMPONE, Francesco

Available from Sheffield Hallam University Research Archive (SHURA) at:

<http://shura.shu.ac.uk/27377/>

This document is the author deposited version. You are advised to consult the publisher's version if you wish to cite from it.

Published version

LENZO, Basilio, ZINGONE, Salvatore Andrea and TIMPONE, Francesco (2020). On the estimation of tyre self-aligning moment through a physical model and the trick tool. *International Journal of Mechanics and Control*, 21 (2), 13-20.

Copyright and re-use policy

See <http://shura.shu.ac.uk/information.html>

ON THE ESTIMATION OF TYRE SELF-ALIGNING MOMENT THROUGH A PHYSICAL MODEL AND THE TRICK TOOL

Salvatore Andrea Zingone^{1,2} Basilio Lenzo¹ Francesco Timpone²

¹Department of Engineering and Mathematics, Sheffield Hallam University, UK

²Department of Industrial Engineering, University of Naples Federico II, Italy

ABSTRACT

The understanding of tyre-road interactions plays a fundamental role in the design of advanced vehicle controllers for enhancing performance and safety. Although there are interesting contributions in the literature that look at estimating tyre-road forces, little has been done on estimating the self-aligning moment. This paper proposes a new method to estimate the self-aligning moment, based on a brush model and a tyre force estimator tool. The idea is that: i) the parameters of a physical model (the brush model) can be optimised to match the lateral forces obtained through a reliable tyre force estimator tool; ii) the optimised model can then be used to compute the self-aligning moment, due to a key feature of the brush model, i.e. that it is a physical model. Hence, unlike other contributions, this method does not require experimental measurements of the self-aligning moment, nor the steering torque. A fitting function is also proposed for the length and width of the contact patch of a tyre as a function of the vertical load. Results show the satisfactory estimation of the lateral force and the consequent self-aligning moment trends, based on experimental manoeuvres carried out on a handling track with a performance-oriented vehicle.

Keywords: vehicle dynamics, tyre-road interaction, self-aligning moment, TRICK tool

1 INTRODUCTION

The investigation of tyre-road interactions plays a key role in vehicle dynamics. Key vehicle design qualities, including safety and performance, can be significantly enhanced with vehicle control techniques based on a thorough understanding of the interaction forces and moments exchanged between tyres and road.

The literature presents several interesting contributions, including different vehicle models and numerous methods to estimate the tyre-road forces [1-5]. On the other hand, little research focuses on the estimation of the self-aligning moment. For instance, [6] proposes a Magic Formula tyre model that can handle inflation pressure changes which includes a formulation for the self-aligning moment, but requires experimental data to fit the model. The work from [7] is also based on the availability of measurements. Direct measurement of tyre-road interaction forces/moments is very challenging. For example it can be achieved through

dedicated sensors, e.g. force/torque transducers, which however are bulky and extremely expensive, hence currently not implementable in common passenger cars.

The self-aligning moment can be inferred by measuring the torque produced by the steering assist motor or by torque sensors mounted on the kingpins [7], yet this is either an uncommon or unpractical feature.

This paper proposes a method to estimate the self-aligning moment without the need of dedicated measurements such as the aforementioned ones. The method is based on a brush model and a procedure that fits the brush model to match the lateral force estimated through a reliable algorithm, i.e. the TRICK (Tyre/Road Interaction Characterization & Knowledge) tool [8-9]. The TRICK tool features a 8-degrees-of-freedom vehicle model that processes experimental signals acquired from a vehicle CAN bus and from sideslip angle measurement or estimation systems, producing force and slip estimates as output. The main idea of the paper is that since the brush model is a physical model, if it can well estimate the lateral force, then it can also be used to calculate the self-aligning moment. Importantly, no experimental data on self-aligning moment are necessary. This is a clear advantage with respect to

Contact author: Basilio Lenzo¹

¹Howard Street, S1 1WB, Sheffield, UK
E-mail: basilio.lenzo@shu.ac.uk

previous approaches, such as the use of well-known Pacejka's Magic Formula, which entails a set of coefficients for each quantity of interest - e.g. lateral force, self-aligning moment etc. - calculated based on corresponding sets of experimental data.

The remainder of this paper is structured as follows. Section II introduces the adopted tyre-road contact model. Section III focuses on the application of such model to the estimation of lateral force and self-aligning moment. Section IV describes the proposed procedure and shows the results obtained on experimental data from a performance car on a handling track. Concluding remarks are in Section V.

2 TYRE-ROAD CONTACT EQUATIONS

The reference frame herein adopted to describe the tyre-road contact is defined according to ISO 8855 [10], as shown in Fig. 1. The origin of the reference frame is in the centre of tyre contact (CTC), and: i) the x axis is the intersection between wheel plane and ground plane, and it has positive direction forward; (ii) the z axis is perpendicular to the ground plane and it has positive direction upward; (iii) the y axis lies on the ground plane, and its direction is chosen to ensure the frame is right-handed. The adopted reference frame has unit vectors $(\underline{e}_x, \underline{e}_y, \underline{e}_z)$.

The tyre-road contact equations are derived through an Eulerian approach. Consider a finite control area $\Gamma(x, y, 0) = \{(x, y, z) \in \mathbb{R}^3: -l/2 \leq x \leq l/2, -b/2 \leq y \leq b/2\}$, in the above-defined reference frame. The contact patch is assumed rectangular (as in many studies, e.g. [11-12]), l and b are respectively its length and width, Fig. 2.

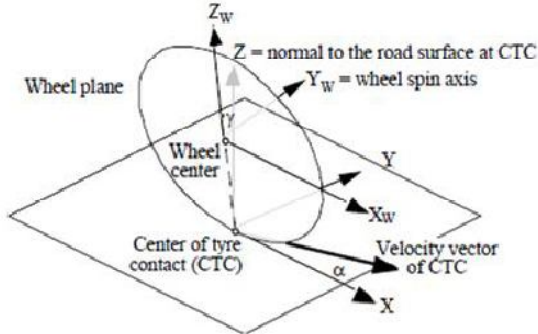


Figure 1. ISO wheel reference system (reproduced from [10]).

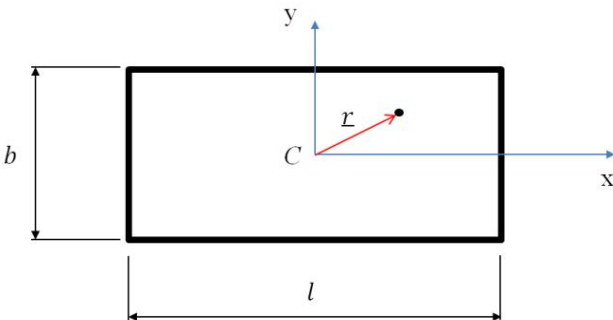


Figure 2. Contact patch and position vector \underline{r} for a generic point.

The vertical dimension is assumed to be zero since the tread only undergoes deformations in the longitudinal and lateral directions. Carcass deformations are neglected. The relative micro-slippage speed between the point of a carcass bristle attached to the rigid body and the one of the tread bristle in contact with the road is

$$\underline{v}(\underline{r}, t) = \underline{V}_s(t) + \omega(t)\underline{e}_z \wedge \underline{r} + \frac{d}{dt}[\underline{u}(\underline{r}, t)] \quad (1)$$

where

- \underline{V}_s is the slippage speed. It is defined as the difference between the speed of the rigid equivalent tyre and that of the road;
- $\omega(t) = \omega_1 - \omega_2$ is the spin angular speed. ω_1 is the normal component of the rolling speed due to camber and ω_2 is the steering speed (attributed to the road);
- $\underline{u}(\underline{r}, t)$ is the displacement field of the tyre tread.

Equation (1) can be rewritten as

$$\underline{v}(\underline{r}, t) = \underline{V}_s(t) + \omega(t)\underline{e}_z \wedge \underline{r} + \frac{\partial \underline{u}(\underline{r}, t)}{\partial \underline{r}} \cdot \frac{d\underline{r}}{dt} + \frac{\partial}{\partial t} \underline{u}(\underline{r}, t) \quad (2)$$

where (for a complete description of the parameters used, the reader is referred to the list of symbols)

$$\frac{d\underline{r}}{dt} = \Omega \underline{e}_y \wedge (-R)\underline{e}_z + \omega_1 \underline{e}_z \wedge \underline{r} \cong -\Omega R \underline{e}_x \quad (3)$$

Assuming steady-state conditions, $\frac{\partial}{\partial t} \underline{u}(\underline{r}, t) = 0$, and by dividing (2) by ΩR , the normalised micro-slippage speed can be defined as

$$\underline{v}^*(\underline{r}, t) = \frac{\underline{v}(\underline{r}, t)}{\Omega R} = \frac{\underline{V}_s(t)}{\Omega R} + \frac{\omega(t)\underline{e}_z}{\Omega} \wedge \frac{\underline{r}}{R} + \frac{\partial \underline{u}(\underline{r}, t)}{\partial \underline{r}} \cdot \frac{-\Omega R \underline{e}_x}{\Omega R} \quad (4)$$

By replacing $\frac{\underline{V}_s(t)}{\Omega R} = \underline{\varepsilon}$ and $\frac{\omega(t)\underline{e}_z}{\Omega} = \psi \underline{e}_z$ in (4):

$$\underline{v}^*(\underline{r}, t) = \underline{\varepsilon} + \psi \underline{e}_z \wedge \frac{\underline{r}}{R} + \frac{\partial \underline{u}(\underline{r}, t)}{\partial \underline{x}} \quad (5)$$

where

$$\underline{\varepsilon} = \begin{bmatrix} \varepsilon_x \\ \varepsilon_y \\ 0 \end{bmatrix} = \frac{1}{\Omega R} \begin{bmatrix} V_x - \Omega R \\ V_y \\ 0 \end{bmatrix} \quad (6)$$

$$\psi \underline{e}_z \wedge \frac{\underline{r}}{R} = \begin{bmatrix} \underline{e}_x & \underline{e}_y & \underline{e}_z \\ 0 & 0 & \psi \\ \frac{x}{R} & \frac{y}{R} & 0 \end{bmatrix} = \frac{\psi}{R} \begin{bmatrix} -y \\ -x \\ 0 \end{bmatrix} \quad (7)$$

$$\underline{u} = \begin{bmatrix} u_x \\ u_y \\ 0 \end{bmatrix} \quad (8)$$

Finally, the components of $\underline{v}^*(\underline{r}, t) = [v_x^* \ v_y^* \ 0]^T$ are

$$v_x^* = \varepsilon_x - \psi \frac{y}{R} - \frac{\partial u_x}{\partial x} \quad (9)$$

$$v_y^* = \varepsilon_y + \psi \frac{x}{R} - \frac{\partial u_y}{\partial x} \quad (10)$$

3 LATERAL INTERACTION AND SELF-ALIGNING MOMENT

The pure lateral interaction problem is studied by assuming a constant value of the slip parameter, ε_y , and assigning $\varepsilon_x = 0, \psi = 0$.

In the adherence zone $v_y^* = 0$, so (10) can be rewritten as

$$\varepsilon_y = \frac{\partial u_y}{\partial x} = \frac{v_{sy}}{\Omega R} = \frac{v_{sy}}{v_x} = \tan \alpha \quad (11)$$

Integrating (11) and imposing the spontaneous entrance condition $U_{y\alpha}^{(a)}(l/2) = 0$, the bristle displacement in adherence condition is

$$U_y^{(a)}(x) = \varepsilon_y x - \frac{\varepsilon_y l}{2} \quad (12)$$

Introducing a new coordinate, $\bar{\xi} = \frac{l-x}{l}$, defined as the dimensionless length from the leading edge (Fig. 3), then (12) can be reformulated as

$$U_y^{(a)}(\bar{\xi}) = -\varepsilon_y \bar{\xi} l \quad (13)$$

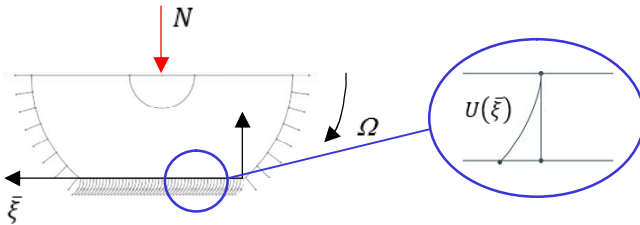


Figure 3. Brush model schematic with indication of some relevant quantities.

From (13), considering the bristle stiffness, the tangential force per unit area acting on the bristle at coordinate $\bar{\xi}$ is

$$\tau_y(\bar{\xi}) = \begin{cases} \tau_y^{(a)} = -k_y \varepsilon_y \bar{\xi} l & \text{if } |\tau_y^{(a)}| \leq \mu_s p(\bar{\xi}) \\ \tau_y^{(s)} = -\mu_d p(\bar{\xi}) \operatorname{sgn}(\varepsilon_y) & \text{if } |\tau_y^{(a)}| > \mu_s p(\bar{\xi}) \end{cases} \quad (14)$$

k_y is the transversal stiffness of the bristle, formally a stiffness per unit area. k_y can be estimated by inverting the following expression, obtainable from $\tau_y^{(a)}$ in (14):

$$\left. \frac{dF_y}{d\varepsilon_y} \right|_{\varepsilon_y=0} = \frac{1}{2} k_y b l^2 \quad (15)$$

where $\left. \frac{dF_y}{d\varepsilon_y} \right|_{\varepsilon_y=0}$ is obtained through the TRICK tool. From

the leading edge, the shear stress increases linearly towards the contact patch. This happens as long as the shear force acting on the bristles is lower than the vertical pressure value multiplied by the static friction coefficient. When they coincide, $\bar{\xi} = \lambda$ is the position of the breakaway point:

$$\tau_y^{(a)}(\bar{\xi}) = -k_y \varepsilon_y \bar{\xi} l = -\mu_s p(\bar{\xi}) \operatorname{sgn}(\varepsilon_y) \quad \text{for } \bar{\xi} = \lambda \quad (16)$$

The transition point between adherence and sliding, defined by the coordinate λ , depends on ε_y . For example, if $\lambda = 0$, the whole contact patch is in sliding conditions.

In this paper, the vertical pressure distribution in the contact patch is a fourth-degree polynomial, satisfying the boundary and the symmetry conditions in the following form [13]:

$$p(\bar{\xi}) = \frac{6N}{bl} A_1 \bar{\xi} (1 - \bar{\xi}) [1 - \bar{\xi} A_2 (1 - \bar{\xi})] \quad (17)$$

where N is the overall wheel normal load (integral of p along the whole contact patch, note that p is constant along y), and $A_1(N)$ and $A_2(N)$ are defined as

$$A_1(N) = \frac{1+a(N)}{1+\frac{a(N)}{5}} \quad (18)$$

$$A_2(N) = \frac{4a(N)}{1+a(N)} \quad (19)$$

$$a(N) = a_0 N / N_0 \quad (20)$$

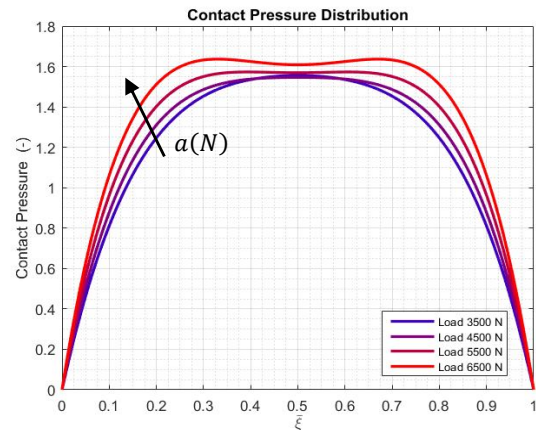


Figure 4. Contact pressure distribution.

The parameter $a(N)$ influences the shape of the contact pressure distribution, e.g. when $a(N) > 1$ the contact pressure function shows a local minimum at $\bar{\xi} = 0.5$, Fig. 4. Note that the pressure distributions in Fig. 4 is obtained for different loads, for which the contact patch area is different. Also, all data presented throughout the paper is normalised due to confidentiality reasons.

The dynamic friction coefficient is considered variable with the slip parameter according to the function shown in Fig. 5. The analytical expression is [14]

$$\mu_d(\varepsilon) = \mu_\infty + \frac{\mu_s - \mu_\infty}{k_1 \varepsilon_y^2 + k_2 |\varepsilon_y| + 1} \quad (21)$$

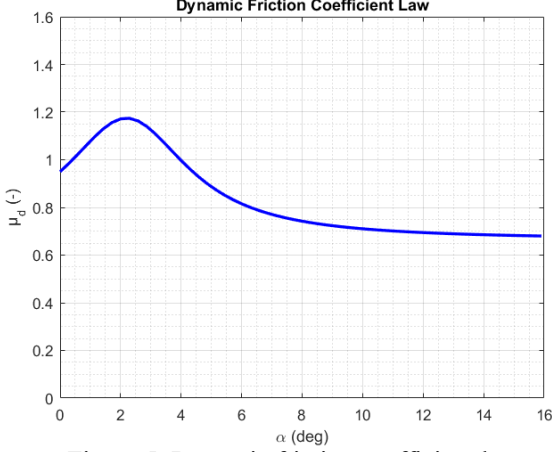


Figure 5. Dynamic friction coefficient law.

The total lateral force developed at the tyre-road interface is calculated by integrating (14) on the contact patch area. Based on (14) being piecewise:

$$F_y = F_y^{(a)} + F_y^{(s)} \quad (22)$$

where $F_y^{(a)}$ is the contribution of the adherence zone and $F_y^{(s)}$ is the contribution of the slippage zone. The first term is

$$F_y^{(a)} = bl \int_0^\lambda \tau_y^{(a)}(\bar{\xi}) d\bar{\xi} \quad (23)$$

By substituting (14) into (23) the adherence force contribution is formulated as

$$F_y^{(a)} = -bl \int_0^\lambda k_y \varepsilon_y \bar{\xi} l d\bar{\xi} \quad (24)$$

The second term of (22) is

$$F_y^{(s)} = -bl \int_\lambda^1 \mu_d p(\bar{\xi}) \cdot \text{sign}(\varepsilon_y) d\bar{\xi} \quad (25)$$

The self-aligning moment is produced because the global lateral force is not applied at the centre of the contact patch:

$$M_z = M_z^{(a)} + M_z^{(s)} \quad (26)$$

where $M_z^{(a)}$ is the moment contribution in the adherence zone and $M_z^{(s)}$ is the moment contribution of the slippage zone. The first term is defined as

$$M_z^{(a)} = bl \int_0^\lambda \tau_y^{(a)}(\bar{\xi}) \left(\frac{1}{2} - \bar{\xi}\right) d\bar{\xi} \quad (27)$$

The second term of (26) is

$$M_z^{(s)} = bl \int_\lambda^1 \tau_y^{(s)}(\bar{\xi}) \left(\frac{1}{2} - \bar{\xi}\right) d\bar{\xi} \quad (28)$$

The self-aligning moment depends on the same physical parameters as the lateral force. So, it can be estimated once such parameters are available, i.e. after tuning the physical parameters on the lateral force dataset, as discussed in the next Section. This is a strength of the proposed approach, which therefore does not require experimental measurements of the self-aligning moment.

4 ESTIMATION PROCEDURE AND EXPERIMENTAL VALIDATION

The developed procedure is based on the knowledge of the estimated tyre-road interaction forces and the contact patch dimensions. As discussed earlier, the tyre-road estimated forces can be obtained via tools such as TRICK [8]. The contact patch dimensions can be obtained by using methods such as those suggested in [15-16]. Here, the TRICK tool was used, while the contact patch dimensions were evaluated using footprint experimental data obtained for different values of normal load. Fig. 6 shows an example of the results obtained, where each footprint was fairly well approximated as a rectangle.

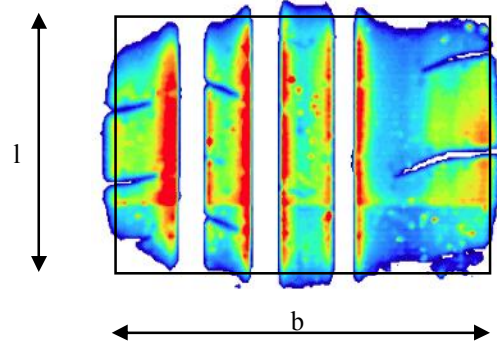


Figure 6. Typical contact patch footprint and rectangular approximation.

Based on the available experimental data, the following functions are proposed to model the contact patch dimensions as functions of the vertical load:

$$l(N) = k_{l1} \tan^{-1}(k_{l2} N) \quad (29)$$

$$b(N) = b_0 + k_{b1} \tan^{-1}(k_{b2} N) \quad (30)$$

Whenever a non-zero vertical load is applied, the width assumes a finite value. Therefore (30) is formally valid for $N > 0$. The coefficients in (29) and (30) were obtained through appropriate fitting tools in Matlab. Results are shown in Fig. 7 and Fig. 8.

Once the interaction forces and the contact patch dimensions are available, the first step of the procedure is the selection of the pure interaction conditions (working points characterized by $\varepsilon_x \cong 0$) within the recorded data. In a second phase a regression algorithm, based on a constrained

nonlinear optimization procedure [17-18], calculates the optimal set of parameters that best fits the lateral force vs slip curves. Specifically the parameters to be optimised are:

- a_0 , which characterises the pressure distribution in (17-20);
- μ_s, μ_∞, k_1 and k_2 , which characterise the dynamic friction coefficient in (21).

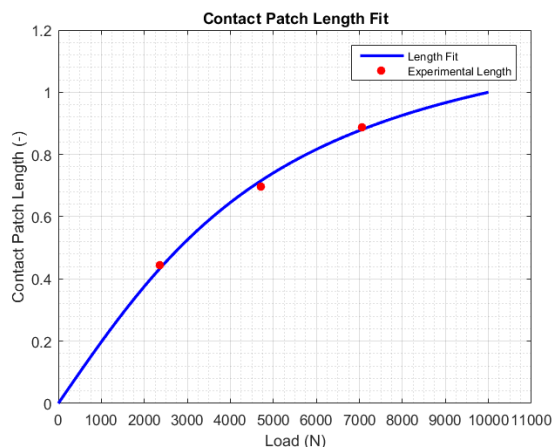


Figure 7. Experimental contact patch length and fitting function (29).

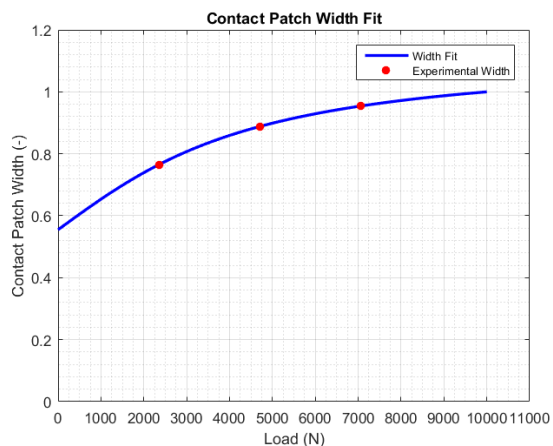


Figure 8. Experimental contact patch width and fitting function (30).

The constraints of the optimisation, for example on the allowed range of the parameters to be optimised, allow their identification based on a physical approach, similar to [19]. For instance, μ_∞ cannot be larger than μ_s .

μ_s is chosen as a constant value for two reasons. First, it is a microscopical parameter that simply represents the friction coefficient between the individual bristle and the road. Secondly, despite μ_s is strictly connected to the peak of the lateral force function which depends on vertical load, the dependence on vertical load is embedded in the brush model. In fact the contact patch area, whose limits are used in the integrations in (22) and (26), is a nonlinear function of the vertical load: it increases less than proportionally [19-20]. μ_s must not be confused with the so-called lateral grip,

defined as $M_y = \frac{F_y}{N}$. Differently from μ_s , M_y is a macroscopical parameter that is commonly a decreasing function of vertical load [21]. As a final remark, unless dedicated test sessions are an option, it is normally uncommon to have operating points near or beyond the lateral force peak. In the present study, data points obtained at large vertical loads provided more sensible information that helped the estimation of μ_s , as shown in Fig. 9.

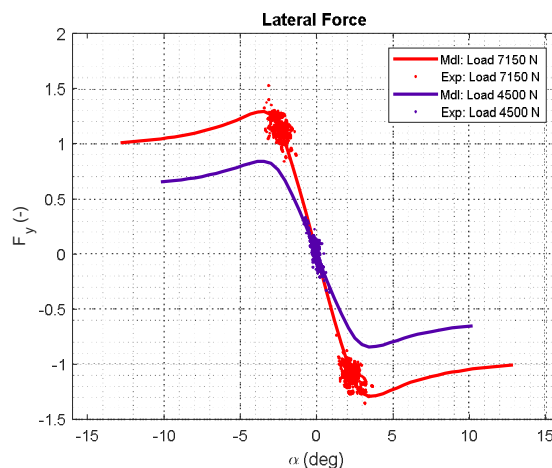


Figure 9. Model ("Mdl") vs experimental ("Exp") lateral force, for a small and a large value of N .

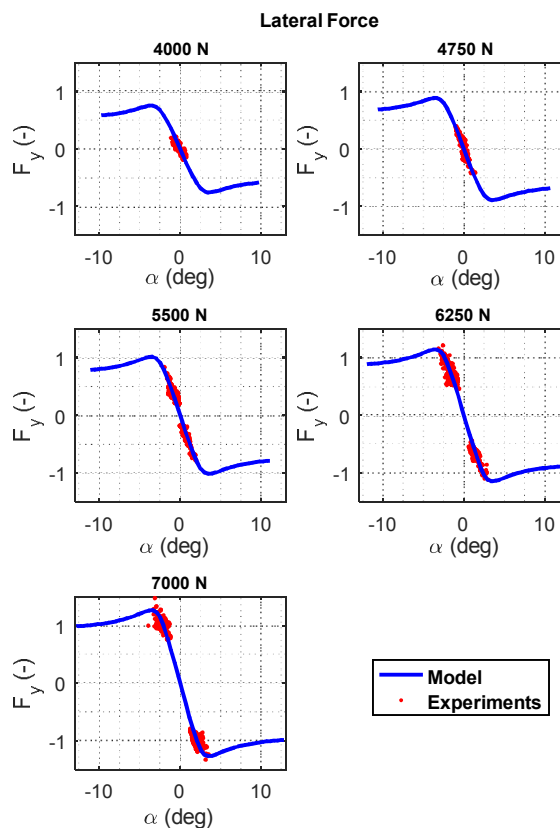


Figure 10. Lateral force: comparison of the estimates from the brush model and from the experimental data.

Overall the procedure led to satisfactory results in terms of lateral force fitting (calibration). Fig. 10 shows a comparison between the optimised brush model and experimental data obtained through TRICK for five values of normal load. Fig. 11 shows the model output for a wider range of normal load. Having validated the brush model on the lateral force, the self-aligning moment can be calculated based on the same physical model, according to (26). The resulting curves are shown in Fig. 12. Sometimes it is preferred to depict the pneumatic trail instead of the self-aligning moment. The pneumatic trail is the distance, along x , between the centre of the contact patch and the point where the total lateral force is applied. The resulting curves are shown in Fig.13.

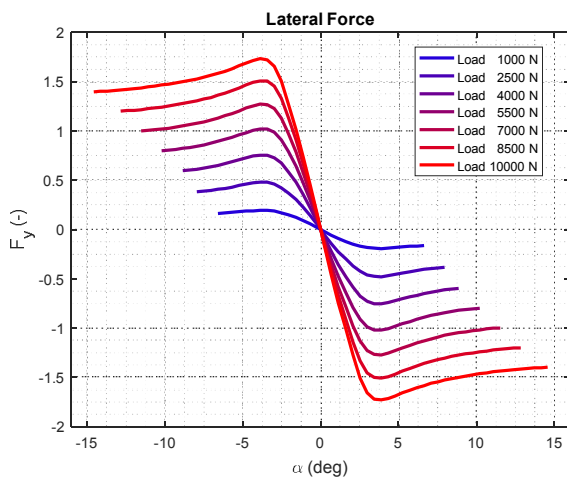


Figure 11. Estimated lateral force.

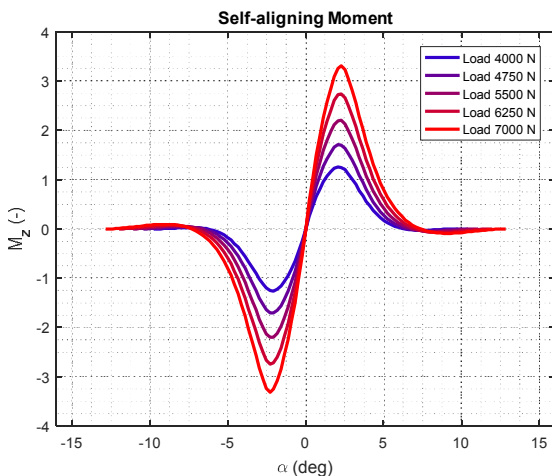


Figure 12. Estimated self-aligning moment.

5 CONCLUSION

This study demonstrated that it is possible to estimate the self-aligning moment for each tyre of a vehicle based on a physical model of the tyre-road interaction, without experimental data on the self-aligning moment. The physical model is deemed reliable as it is tuned to fit the

experimental lateral force behaviour, which can be obtained through advanced tools such as TRICK.

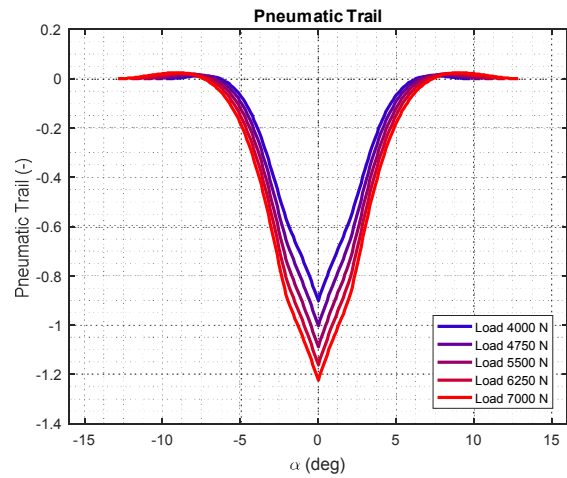


Figure 13. Estimated pneumatic trail.

Future studies are to entail an experimental validation on a dedicated test bench, and the extension of the model to include the combined (longitudinal-lateral) tyre-road interaction. Further investigations will also involve the integration of this method within advanced vehicle control techniques, which need accurate knowledge of the tyre-road interaction actions. This is also a basic requirement for autonomous vehicles, which require a deep understanding of the surrounding environment - but that comes after the full knowledge of the behaviour of the controlled vehicle.

REFERENCES

- [1] M. Acosta, S. Kanarachos. Tire lateral force estimation and grip potential identification using Neural Networks, Extended Kalman Filter, and Recursive Least Squares, *Neural Computing and Applications*, 30(11), pp.3445-3465, 2018.
- [2] A. Rezaeian, R. Zarringhalam, S. Fallah, W. Melek, A. Khajepour, S. Chen, et al. Novel tire force estimation strategy for real-time implementation on vehicle applications, *IEEE Transactions on Vehicular Technology*, 64(6), 2231-2241, 2014.
- [3] W. Cho, J. Yoon, S. Yim, B. Koo, K. Yi. "Estimation of tire forces for application to vehicle stability control, *IEEE Transactions on Vehicular Technology*, 59(2), pp.638-649, 2009.
- [4] A. Albinsson, F. Bruzelius, M. Jonasson, B. Jacobson. "Tire force estimation utilizing wheel torque measurements and validation in simulations and experiments, *12th International Symposium on Advanced Vehicle Control (AVEC'14), Tokyo Japan*, pp. 294-299, 2014.
- [5] G. Napolitano Dell'Annunziata, B. Lenzo, F. Farroni, A. Sakhnevych, F. Timpone. A New Approach for Estimating Tire-Road Longitudinal Forces for a Race Car, *IFTOMM World Congress on Mechanism and*

- Machine Science* (pp. 3601-3610), Springer, Cham, 2019.
- [6] I. J. M. Besselink, A. J. C. Schmeitz, H. B. Pacejka. An improved Magic Formula/Swift tyre model that can handle inflation pressure changes, *Vehicle System Dynamics*, 48(S1), pp.337-352, 2010.
- [7] S. Song, M. C. K. Chun, J. Huissoon, S. L. Waslander. Pneumatic trail based slip angle observer with Dugoff tire model, *2014 IEEE Intelligent Vehicles Symposium Proceedings* (pp. 1127-1132), 2014.
- [8] F. Farroni. TRICK Tire/Road Interaction Characterization & Knowledge - A tool for the evaluation of tire and vehicle performances in outdoor test sessions, *Mechanical Systems and Signal Processing*, 72, pp. 808-831, 2016.
- [9] G. Napolitano Dell'Annunziata, B. Lenzo, A. Sakhnevych, F. Farroni, F. Timpone, M. Barbieri. Towards TRICK 2.0 – A tool for the evaluation of the vehicle performance through the use of an advanced sensors system, *Conference of the Italian Association of Theoretical and Applied Mechanics*, pp. 1093-1102, Springer, Cham, 2019.
- [10] ISO 8855:2011, Road vehicles "Vehicle Dynamics and Road-Holding Ability", Vocabulary, 1992.
- [11] J. Yi, L. Alvarez, X. Claeys, X., R. Horowitz. Emergency braking control with an observer-based dynamic tire/road friction model and wheel angular velocity measurement, *Vehicle system dynamics*, 39(2), 81-97, 2003.
- [12] T. Akasaka, M. Katoh, S. Nihei, M. Hiraiwa. Two-dimensional contact pressure distribution of a radial tire, *Tire Science and Technology*, 18(2), 80-103, 1990.
- [13] G. Capone, D. Giordano, M. Russo, M. Terzo, F. Timpone. Ph.An.Ty.MHA: a physical analytical tyre model for handling analysis—the normal interaction, *Vehicle System Dynamics*, 47(1), pp. 15-27, 2009.
- [14] L. Romano, A. Sakhnevych, S. Strano, F. Timpone. A novel brush-model with flexible carcass for transient interactions, *Meccanica*, 54(10), pp. 1663-1679, 2019.
- [15] F. Braghin, M. Brusarosco, F. Cheli, A. Cigada, S. Manzoni, F. Mancosu. Measurement of contact forces and patch features by means of accelerometers fixed inside the tire to improve future car active control, *Vehicle System Dynamics*, 44(sup1), pp.3-13, 2006.
- [16] N. Roveri, G. Pepe, A. Carcaterra. OPTTYRE—A new technology for tire monitoring: Evidence of contact patch phenomena, *Mechanical Systems and Signal Processing*, 66, pp.793-810, 2016.
- [17] A. Amoresano, G. Langella, V. Niola, G. Quaremba. Statistical method to identify the main parameters characterizing a pressure swirl spray, *International Review of Mechanical Engineering (IREME)*, 7(6), pp. 1007-1013, 2013.
- [18] R.H. Byrd, J.C. Gilbert, J. Nocedal. A Trust Region Method Based on Interior Point Techniques for Nonlinear Programming, *Mathematical Programming*, 89(1), pp. 149–185, 2000.
- [19] F. Farroni, M. Russo, A. Sakhnevych, F. Timpone. An Application of TRIP-ID: MF Identification Tool for an Automobile Tire Interaction Curves Dataset, *2nd International Conference of IFToMM ITALY*, Springer International Publishing, pp. 100-113, 2019.
- [20] A. N. Gent, J. D. Walter. The Pneumatic Tire, University of Akron, National Highway Traffic Safety Administration (NHTSA), 2006.
- [21] M. Guiggiani. *The science of vehicle dynamics*. 2nd edition, Springer International Publishing, 2018.

LIST OF SYMBOLS

Symbol	Quantity
$a(N)$	Contact pressure coefficient
a_0	Static load contact pressure coefficient
b	Width of the contact patch
b_0	Coefficient of the contact patch width law
\underline{e}_x	Unit vector for axis x
\underline{e}_y	Unit vector for axis y
\underline{e}_z	Unit vector for axis z
F_y	Lateral force
$F_y^{(a)}$	Adherence lateral force contribution
$F_y^{(s)}$	Sliding lateral force contribution
$k(N)$	Scaling factor of contact pressure coefficient
k_{b1}, k_{b1}	Coefficients of the contact patch width law
k_{l1}, k_{l2}	Coefficients of the contact patch length law
k_y	Transversal stiffness of the bristle
k_1, k_2	Coefficients of the dynamic friction law
l	Length of the contact patch
M_z	Self-aligning moment
$M_z^{(a)}$	Adherence self-aligning moment contribution
$M_z^{(s)}$	Sliding self-aligning moment contribution
N	Normal load on the wheel
N_0	Reference value of wheel normal load
p	Contact pressure
P	Position of a generic point of a carcass bristle
\underline{r}	Vector position in the x-z plane

R	Pure rolling radius	ω_1	Normal component of the rolling speed
t	Time	ω_2	Steering speed
$\underline{u}(\underline{r}, t)$	Displacement field of a tread bristle	Ω	Component of the rolling speed parallel to the road
$U_y^{(a)}$	Displacement of a tread bristle in they-direction in adherence condition		
$\underline{v}(\underline{r}, t)$	Speed of a point of a tread bristle		
$\underline{v}^*(\underline{r}, t)$	Nondimensional speed of a point of a tread bristle		
v_x^*	Nondimensional longitudinal speed of a point of a tread bristle		
v_y^*	Nondimensional lateral speed of a point of a tread bristle		
$\underline{V}_s(t)$	Global slippage speed		
V_{sx}	Global longitudinal slippage speed		
V_{sy}	Global lateral slippage speed		
V_x	Wheel centre longitudinal speed		
V_y	Wheel centre lateral speed		
x	Axis defined as the intersection of the wheel plane and the ground plane		
y	Axis on the ground plane, perpendicular to x		
z	Axis perpendicular to the ground plane		
α	Slip angle		
Γ	Control area		
$\underline{\varepsilon}$	Slip parameter		
ε_x	Longitudinal slip parameter		
ε_y	Lateral slip parameter		
λ	Dimensionless coordinate of the breakaway point		
μ_s	Static friction coefficient of the bristle		
μ_d	Dynamic friction coefficient of the bristle		
μ_∞	Asymptotical value of the dynamic friction coefficient of the bristle		
M_y	Lateral grip		
$\bar{\xi}$	Dimensionless coordinate from the leading edge		
τ_y	Shear stress along y		
$\tau_y^{(a)}$	Shear stress along y in adherence condition		
$\tau_y^{(s)}$	Shear stress along y in sliding condition		
ψ	Spin parameter		
$\omega(t)$	Spin speed		